UC San Diego
International Symposium on Stratified Flows

Title
Damping of 3D internal wave attractors by lateral walls

Permalink

Journal

Authors
Beckebanze, Felix
Maas, Leo

Publication Date
2016-08-29

Damping of 3D internal wave attractors by lateral walls

Felix Beckebanze[1] and Leo R. M. Maas[2]

[1]Mathematical Institute, Utrecht University, Netherlands
[2]Institute for Marine and Atmospheric Research, Utrecht University, Netherlands
f.beckebanze@uu.nl

Abstract

The reflection of internal gravity waves at sloping boundaries leads to focusing or defocusing. In closed domains, focusing dominates and projects the wave energy onto 'wave attractors'. Previous theoretical and experimental work on 2D steady state wave attractors has demonstrated that geometric focusing by wave reflection can be balanced either by viscous dissipation at high wave numbers (Hazewinkel et al., 2008), or by nonlinear wave-wave interactions (Scolan et al., 2013).
The present study considers a weakly nonlinear 3D internal wave beam under steady state conditions in a semi-infinite domain between two vertical walls. We analyze the effect of the Stokes boundary layers at these two vertical side walls on the interior velocity field. With a perturbation approach, we find that the two lateral Stokes boundary layers generate a fully three-dimensional interior velocity field component, proportional to $\nu^{1/2}$, with ν the dynamical viscosity. This velocity field dampens the wave beam at high wave numbers, thereby providing a new mechanism to establish an energetic balance for steady state wave attractors. The analytical results agree well with the 3D numerical wave attractor simulation by Brouzet et al. (2016).

1 Introduction

The dispersion relation of internal waves is given by $\omega_0^2 = N_0^2 \sin^2 \theta$, with ω_0 the wave frequency, θ the angle of phase propagation with respect to the vertical, z, antiparallel to gravity, and N_0 the Brunt-Väisälä frequency, assumed constant. The group propagation is always orthogonal to the phase propagation (Sutherland, 2010), thus the angle of energy radiation with respect to the vertical is fixed for monochromatic waves. This property results in geometric focusing or defocusing upon reflection at sloping topography. Repeated geometric focusing in closed domains can project the wave energy onto closed orbits, known as wave attractors (Maas and Lam, 1995; Maas et al., 1997). In the vicinity of the wave attractor, energy is dissipated by viscous dissipation (Hazewinkel et al., 2008; Rieutord et al., 2002), or lost to nonlinear wave-wave interactions (Scolan et al., 2013). The energy loss at the wave attractor can have far-reaching consequences for the mixing budget of stratified fluids, such as the oceans.
Hazewinkel et al. (2008) studied the equilibrium spectrum of internal wave attractors in the classical trapezoidal set-up, both in the laboratory and with a simple model. For their model, the nonlinearity is assumed to be negligibly small, and the energy input is taken at low wave numbers. The geometric focusing increases the wave numbers k by the factor

$$\gamma = \frac{\sin(\alpha + \theta)}{\sin(\alpha - \theta)} > 1$$

upon each reflection at the supercritically inclined wall (of angle $\alpha > \theta$ with respect to the horizontal). Let $A(k)$ be the wave number spectrum of the buoyancy gradient, $\partial_\eta b$,

with η normal to the wave attractor. For the spectrum $A(k)$, the focusing leads to a linear increase[1], i.e.

$$A(\gamma k) = \gamma A(k).$$

For each loop along the wave attractor with length L_a, the propagating internal waves are dampened with the factor[2] $\exp[-\frac{L_a \nu \tan\theta}{2\omega_0} k^3]$, with ν the dynamical viscosity. The balance between the geometric focusing and viscous dissipation sets the width of the wave attractor.

In this study, we extend the simple model by Hazewinkel et al. (2008) by incorporating the damping induced by two Stokes boundary layers at the lateral walls. In §2 we construct the 3D velocity field of an internal wave beam between two walls, representing one branch of an attractor. We show that our analytical three-dimensional velocity field corresponds well with the the 3D numerical wave attractor simulation by Brouzet et al. (2016). Subsequently, in §3, we determine the damping exerted by the two boundary layers on an internal wave attractor. Additionally, we compare the theoretical equilibrium spectrum of our extended model with the observed wave attractor spectrum by Hazewinkel et al. (2008). Conclusions are drawn in §4. Our results establish that the three-dimensionality of the typical, semi-2D laboratory set-ups are not negligible for the shape of the wave attractor, contrary to what was previously thought.

2   Internal wave beam between lateral walls

To study the effect of the no-slip boundary conditions at two lateral walls on an internal wave beam, we consider an infinite domain with Cartesian coordinates (x, y, z) between two walls at $y = \pm h$. The linearized equations governing the dimensionless velocity field $\mathbf{u} = (u, v, w)$, buoyancy b, and pressure p of the Boussinesq fluid, with scaled Brunt-Väisälä frequency $N = N_0/\omega_0$, are given by

$$\mathbf{u}_t = -\nabla p + \delta^2 \Delta \mathbf{u} + b\hat{z}, \qquad b_t = -N^2 w, \qquad \nabla . \mathbf{u} = 0. \tag{1}$$

Here, $\delta = \frac{d_0}{L_0} \ll 1$ is the thickness of the boundary layer, $d_0 = \sqrt{\nu/\omega_0}$, scaled with the typical thickness of the wave beam, L_0. We solve (1) with no-slip boundary conditions $\mathbf{u} = \mathbf{0}$ at $y = \pm h$ by expanding the velocity vector $\mathbf{u}$ in the small parameter δ,

$$\mathbf{u} = \mathbf{u}_0 + \delta \mathbf{u}_1 + \mathcal{O}(\delta^2),$$

and similarly for buoyancy b and pressure p. We assume that $h = H/L_0 \geq 1$, i.e. the dimensional width of the domain, $2H$, is at least of the same order of magnitude as the wave beam width, L_0.

We restrict the energy propagation to be upwards along $\xi = x\cos\theta + z\sin\theta$, implying that the phase propagation is downwards along negative $\zeta = -x\sin\theta + z\cos\theta$. Using these constraints, the most general wave beam velocity field at $y = 0$, solving (1) at $\mathcal{O}(\delta^0)$, is given by

$$[u_0, v_0, w_0] = [\cos\theta, 0, \sin\theta]U, \qquad \text{with } U = -i \int_0^\infty \frac{A(k)}{k\sin\theta} e^{i(k\zeta+t)-\delta\beta\xi} dk, \tag{2}$$

---

[1]We have corrected for a missing factor γ^{-1} on the right-hand side of the recursxive relation $A_n^2 = \gamma^3 A_{n-1}^2$ by Hazewinkel et al. (2008), where A_n and A_{n-1} are the buoyancy gradient spectra before and after reflection, respectively.

[2]In the viscous dissipation decay rate, we also corrected for a missing factor $1/2$ in Hazewinkel et al. (2008).

for some undetermined, complex-valued β, and k now dimensionless (scaled by L_0^{-1}). We claim that $\beta \in \mathcal{O}(1)$, implying that $U_\xi \in \mathcal{O}(\delta)$, thus the along-wave-beam velocity component U is divergent at $\mathcal{O}(\delta)$. It is the real part of $\delta\beta$, which describes the damping of the interior wave beam due to the presence of the two lateral Stokes boundary layers. The purpose of the present analysis is to determine β. In §3 we solve for β by matching the divergence U_ξ at $\mathcal{O}(\delta)$, with the divergence of the $\mathcal{O}(\delta)$-transversal velocity component, v_1, which is determined next.

Using the stretched coordinate $\eta = \delta^{-1}y$, the momentum equations for u_0 and w_0 are given by

$$iu_0 = -p_{0_x} + u_{0_{\eta\eta}}, \quad -i\cot^2\theta\, w_0 = -p_{0_z} + w_{0_{\eta\eta}}. \tag{3}$$

In these two equations, the partial time derivatives have already been replaced by i. It is the buoyancy, $b_0 = i\sin^{-2}\theta\, w_0$, which adds to the time derivative of the vertical velocity component, producing the factor $-\cot^2\theta$. The along-wave-beam velocity component U is related to the pressure gradient in η-direction by $p_{0_\eta} = i\cot\theta U$. Solving (3) with no-slip boundary conditions at the walls, $\eta = \pm\delta^{-1}h$, and prescribed velocity field (2) in the center plane, $\eta = 0$, gives

$$u_0 = \cos\theta\left(1 - \frac{\cosh[i^{\frac{1}{2}}\eta]}{\cosh[i^{\frac{1}{2}}\delta^{-1}h]}\right)U, \quad w_0 = \sin\theta\left(1 - \frac{\cosh[i^{-\frac{1}{2}}\cot\theta\eta]}{\cosh[i^{-\frac{1}{2}}\cot\theta\delta^{-1}h]}\right)U. \tag{4}$$

The presence of stratification (non-zero buoyancy) causes the factor-$\cot\theta$ difference in the thicknesses of the boundary layer, δ and $\delta\tan\theta$, for respectively horizontal and vertical velocity components, making $(u_0, 0, w_0)$ divergent near the walls. In Fig. 1a,b these velocity components are compared with the 3D numerical simulation by Brouzet et al. (2016). During the (non-steady) start-up phase, the numerical data (blue circles) fit the analytical velocity components (green lines) remarkably well. At steady state (red circles), the boundary layer structure is also well-captured by our analytical velocity expression (4). The discrepancy between numerical data and exact expressions towards the center, $y = 0$, hints at the presence of some 3D effect in the interior, outside of the boundary layers, which is not captured by (4).

By the continuity equation at $\mathcal{O}(\delta^0)$ in stretched coordinate, η,

$$u_{0_x} + w_{0_z} = -v_{1_\eta},$$

we get the $\mathcal{O}(\delta)$ transversal velocity component[3]

$$v_1 = \sin\theta\cos\theta\left(i^{\frac{1}{2}}\tan\theta\frac{\sinh[i^{-\frac{1}{2}}\cot\theta\eta]}{\cosh[i^{-\frac{1}{2}}\cot\theta\delta^{-1}h]} - i^{-\frac{1}{2}}\frac{\sinh[i^{\frac{1}{2}}\eta]}{\cosh[i^{\frac{1}{2}}\delta^{-1}h]}\right)U_\zeta + V(y).$$

Here, $V(y)$ is an undetermined velocity component satisfying $V_y(y) \in \mathcal{O}(\delta)$, that is to say, slowly varying in y-direction. The impermeability boundary condition ($v_1 = 0$) at both walls translates to

$$V(\pm h) = \pm\sigma U_\zeta, \quad \text{with} \tag{5}$$

$$\sigma = \sin\theta\cos\theta\left(i^{-\frac{1}{2}}\tanh[i^{\frac{1}{2}}\delta^{-1}h] - i^{\frac{1}{2}}\tan\theta\tanh[i^{-\frac{1}{2}}\cot\theta\delta^{-1}h]\right).$$

---

[3]The y-momentum equation is also satisfied at $\mathcal{O}(\delta)$ by choosing an appropriate pressure $p_2(\eta)$, which is $\mathcal{O}(\delta^2)$, thus negligible.
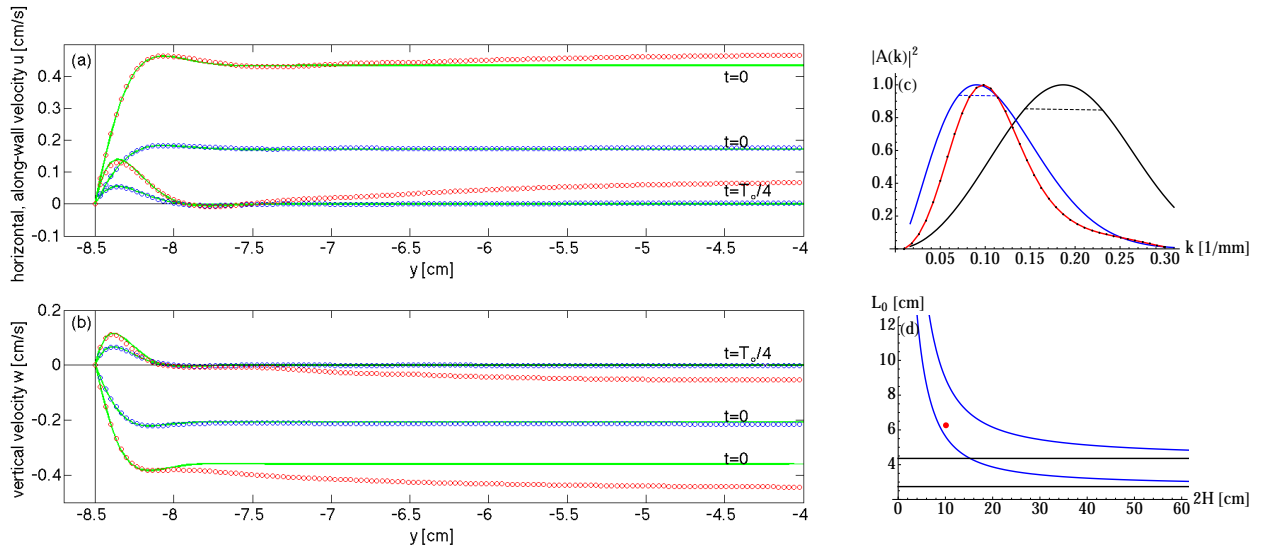
Figure 1: Horizontal velocity u (a) and vertical velocity w (b) at two points in time, $t = 0$ and $t = T_0/4$, with $T_0 = 2\pi/\omega_0$ the period. Circles: numerical simulation by Brouzet et al. (2016), filtered around $\omega_0 = 0.589 s^{-1}$ over respectively 3 T_0 during start-up phase (blue), and over 75 periods during steady state (red). Green lines: the analytical expressions (4) for u_0 and w_0, with their amplitudes fitted to the corresponding numerical data at $t = 0$ and $y = -8.1$ cm. In (c), the (normalized) observed spectrum $|A(k)|^2$ (red) by Hazewinkel et al. (2008) is compared with the theoretical spectrum, expression (6) for $P = constant$, with (blue) and without (black) wall damping. The ranges $[k_b, \gamma k_b]$ for the peak for all possible choices of P are indicated by the horizontal dashed lines. Plot (d) shows the range $2\pi/k_b[\gamma^{-1}, 1]$ (between blue lines) as a function of tank width, $2H$; the black horizontal lines present the same range for internal viscous dissipation only ($H \to \infty$). The observed attractor width, L_0, in the experiment by Hazewinkel et al. (2008) is indicated by the red dot. We refer to the cited papers for the details on the 3D simulation and laboratory set-up, including the parameter values, which we adopted.

In the limit $\delta^{-1}h \gg 1$, the expression simplifies to $\sigma = \sin\theta e^{-i(\theta+\pi/4)}$. The transversal velocity component V is governed by (1) at $\mathcal{O}(\delta)$ in the unstretched coordinates, (x, y, z). The continuity equation at $\mathcal{O}(\delta)$ reads $U_\xi + V_y = 0$. Since U is y-independent, we get $V_{yy} = 0$, hence $V = \frac{\sigma y}{h}U_\zeta$. Thus, the transversal velocity v decays linearly (= slowly) towards the center plane, $y = 0$, making the velocity field in the interior truly three-dimensional at $\mathcal{O}(\delta h^{-1})$.

3   Damping by lateral walls

Rewriting the continuity equation $U_\xi + V_y = 0$ in terms of the spectrum $A(k)$ gives

$$\int_0^\infty \left(i\frac{\sigma\delta}{h}k - \delta\beta \right) \frac{A(k)}{k} e^{i(\zeta k+t)-\delta\beta\xi} dk = 0.$$

This equation is satisfied for an arbitrary spectrum $A(k)$ if and only if

$$\beta = \frac{i\sigma k}{h}.$$

Hence, the velocity U decays in the along-wave-beam direction, ξ, with $e^{-\delta h^{-1}\sigma_0 k\xi}$, where $\sigma_0 = \Re[i\sigma] > 0$ for $\theta \in (0, \pi/2)$. The imaginary part of β, which takes both positive and negative values for $\theta \in (0, \pi/2)$, describes a slight change in tilt in phase propagation direction, that changes from ζ to $\zeta - \delta h^{-1}\Re[\sigma]\xi$.

We now turn to the simple model for the equilibrium spectrum $A(k)$ by Hazewinkel et al. (2008), which we briefly introduced in §1 (with k again dimensional). Our extended model for the wave spectrum $A(k)$, incorporating both internal viscous dissipation and the damping by the two lateral walls, gives the constraint

$$A(\gamma k) = \gamma A(k) \exp\left[-\frac{L_a d_0 i\sigma}{H}k - \frac{L_a d_0^2 \tan\theta}{2}k^3\right]. \tag{6}$$

Solutions to (6) are not unique. All solutions to the inviscid case, $A(\gamma k) = \gamma A(k)$, are given by $kP(\log_\gamma(k))$ for arbitrary period-1 functions P (Beckebanze and Keady, 2016). Extending this to (6) gives

$$A(k) = kP(\log_\gamma(k))e^{-\lambda_1 k - \lambda_2 k^3}, \quad \text{with } \lambda_1 = \frac{iL_a d_0 \sigma}{H(\gamma-1)} \text{ and } \lambda_2 = \frac{L_a d_0^2 \tan\theta}{2(\gamma^3-1)}. \tag{7}$$

The "model continuous" by Hazewinkel et al. (2008) corresponds to $P = constant$. Whereas the corrected[4] theoretical spectrum by Hazewinkel et al. (2008) (black line in Fig. 1c) clearly mismatches the observed spectrum (red line), the extended theoretical spectrum (blue line) matches the observation fairly well.

The choice $P = constant$ is arbitrary, and different choices for the period-1 function P lead to different wave numbers k_0 for which $|A(k)|$ peaks. The maximum of $|A(k)|$ for arbitrary period-1 function P falls in the range $(k_b, \gamma k_b)$, where $k_b > 0$ solves $|A(k_b)| = |A(\gamma k_b)|$ for $P = constant$. This range is indicated by the horizontal dashed lines in Fig. 1c. Consequently, without knowledge of the precise energy input at low wave numbers, one can only define a range for the typical thickness of the wave attractor, $L_0 = \frac{2\pi}{k_0}$, as indicated Fig. 1d.

4   Conclusions and discussion

The present analysis establishes the importance of damping by the lateral walls on the shape of wave attractors in semi-2D set-ups. Neglecting the effects by the side walls ($H \to \infty$), we get a viscous attractor width[5] $L_0^I = 2\pi(3\lambda_2)^{1/3} \propto (L_a\nu/N_0)^{1/3}$, as originally found by Rieutord et al. (2001) and numerically verified by Grisouard et. al. (2008). Damping only by the walls results in an attractor width $L_0^W = 2\pi\Re[\lambda_1] \propto (L_a/H)(\nu/N_0)^{1/2}$. Interestingly, this attractor width, L_0^W, is independent of the actual size of the 3D tank, because scaling both L_a and H leaves L_0^W invariant. The effects of the walls may be neglected only if $L_0^I \gg L_0^W$, which is the case when

$$H \gg L_a^{2/3}d_0^{1/3}\sigma_0[\cot\theta\, 2(\gamma^3-1)/3]^{1/3}/(\gamma-1).$$

For the experiments by Maas et al. (1997), Hazewinkel et al. (2008), and Brouzet et al. (2016), this is not the case.

Recall that it is the stratification, which causes the factor-$\cot\theta$ difference in the thicknesses

---

[4]Notice that the spectrum for internal dissipation only (black line in our Fig. 1c) does not correspond to the same theoretical spectrum in Hazewinkel et al. (2008), their Fig. 6, because they seemingly scaled their set of wave numbers, $\{k_0, k_1, k_2, ...\}$, while keeping the corresponding spectrum amplitudes, $\{A_0, A_1, A_2, ...\}$, constant. However, all amplitudes A_n, $n = 0, 1, 2, ...$ depend on k_0. Strictly speaking, it is thus not permitted to change k_0 without adjusting A_n. Additionally, we corrected for the missing factors γ^{-1} and $\frac{1}{2}$ discussed in footnotes 1 and 2.

[5]For simplicity, we consider only $P = constant$.

of the Stokes boundary layer for vertical and horizontal velocity components. Vasiliev and Chashechkin (2003) also found this peculiar twist of the stratification on the boundary layer thickness in their theoretical study on 3D internal wave generation by an oscillating inclined plane.

While the boundary layer structure of our analytical velocity expressions fits the numerical data by Brouzet et al. (2016) very well, the comparison also reveals some discrepancies for the steady state motion. It appears that our assumption that, away from the boundaries, the along-wave-attractor velocity does not vary in transverse direction ($U_y = 0$ in the interior) does not hold. Through the non-linear advection terms, a mean flow and the first higher harmonic are induced at lowest order of (weak) non-linearity. It is speculated that these flow components might interact with the leading-order monochromatic velocity field, thereby producing the numerically observed inhomogeneity in the harmonic field in the transversal direction (Fig. 1a,b).

References

Beckebanze, F. and Keady, G. (2016). On functional equations leading to exact solutions for standing internal waves. *Wave Motion*, 60:0-15.

C. Brouzet, I. Sibgatullin, H. Scolan, E. V. Ermanyuk, T. Dauxois (2016). Internal wave attractors examined using laboratory experiments and 3D numerical simulations. *J. Fluid Mech.*, 793:109-131.

Grisouard, N., Staquet, C. and Pairaud, I. (2008). Numerical simulation of a two-dimensional internal wave attractor. *J. Fluid Mech.*, 614:1-14.

Hazewinkel, J., van Breevoort, P., Dalziel, S.B. , Maas, L. R. M. (2008). Observations on the wave number spectrum and evolution of an internal wave attractor, *J. Fluid Mech.*, 598:373-382.

Maas, L. R. M. and Lam, F.-P. A. (1995). Geometric focusing of internal waves. *J. Fluid Mech.*, 300:1-41.

Maas, L. R. M., Benielli, D., Sommeria, J. and Lam, F.-P. A. (1997). Observation of an internal wave attractor in a confined, stably stratified fluid. *Nature*, 388:557-561.

Rieutord, M., Georgeot, B. and Valdettaro, L. (2001). Inertial waves in a rotation spherical shell: attractors and asymptotic spectrum. *J. Fluid Mech.*, 435:103-144.

Rieutord, M., Valdettaro, L. and Georgeot, B. (2002). Analysis of singular inertial modes in a spherical shell: the slender toroidal shell mode. *J. Fluid Mech.*, 463:345-360.

Scolan, H., Ermanyuk, E. V., Dauxois, T. (2013). Nonlinear fate of internal wave attractors. *Phys. Rev. Lett.*, 110, 234501.

Sutherland, B. R. (2010). Internal Gravity Waves. *Cambridge University Press*, ISBN: 978-0-521-83915-0.

Vasiliev, A. Y. and Chashechkin, Y. D. (2003). Generation Of 3d Periodic Internal Wave Beams. *J. Appl. Mathes Mechs*, 67:397-405.